Towards physical descriptors of active and selective catalysts for the oxidation of n-butane to maleic anhydride

Maik Eichelbaum,[*,†] Robert Glaum,[‡] Michael Hävecker,[†,¶] Knut Wittich,[‡] Christian Heine,[†] Heiner Schwarz,[†] Cornelia-Katharina Dobner,[§] Cathrin Welker-Nieuwoudt,[§] Annette Trunschke,[†] and Robert Schlögl[†]

Department of Inorganic Chemistry, Fritz-Haber-Institut der Max-Planck-Gesellschaft, Faradayweg 4-6, 14195 Berlin, Germany, Institut für Anorganische Chemie, Universität Bonn, Gerhard-Domagk-Straße 1, 53121 Bonn, Germany, Solar Energy Research, Helmholtz-Zentrum Berlin / BESSY II, Albert-Einstein-Straße 15, 12489 Berlin, Germany, and Chemicals Research and Engineering, BASF SE, Carl-Bosch-Straße 38, 67056 Ludwigshafen, Germany

E-mail: me@fhi-berlin.mpg.de

Phone: +49 (0)30 84134566. Fax: +49 (0)30 84134401

Abstract

Based on our newly developed microwave cavity perturbation technique the microwave conductivity of diverse vanadium (III), (IV) and (V) phosphate catalysts is measured under reaction conditions for the selective oxidation of n-butane. The conductivity response on the gas

[*]To whom correspondence should be addressed
[†]Fritz-Haber-Institut
[‡]Universität Bonn
[¶]Helmholtz-Zentrum Berlin
[§]BASF SE

phase is identified as very sensitive measure for the redox kinetics, reversibility and stability of the samples, which are important prerequisites for highly selective and active catalysts. The sensitivity achieved by our method is comparable to surface-sensitive methods such as X-ray photoelectron spectroscopy, whereas more conventional analytics such as X-ray diffractometry or Raman spectroscopy only indicate the stability of the bulk crystal phase under the same reaction conditions.

Introduction

Heterogeneously catalyzed selective oxidation reactions are of particular importance for our society, since 25% of all industrial organic chemicals and intermediates are produced this way.[1,2] In this contribution we will focus on the selective oxidation of n-butane to maleic anhydride (MA) over vanadium phosphorus oxides. This reaction was the first example of a commercially applied selective oxidation of an alkane to produce a bulk chemical,[3] and hence is of both academic and industrial relevance. The partial oxidation to MA is catalyzed by chemically relatively simple and homogeneous compounds such as the industrially used phase-pure vanadyl pyrophosphate $(VO)_2P_2O_7$ (VPP). Accordingly, the bulk properties of the material are very well known making it an ideal system for the investigation of the working mode of a high-performance catalyst. However, despite tedious optimization attempts, VPP only allows MA yields not higher than 65 mol%. Albeit the great effort made in studying this catalyst, the atomic or electronic surface structure, and in particular the reason for VPP being such a unique (though not perfect) catalytic system, e.g. in comparison to alternative vanadium phosphorus oxides, is still a matter of intense debates.[4–13]

Very often the working mode of VPP is described as Mars-van-Krevelen (MvK) mechanism (or the kinetics by the MvK rate-expression).[4,5,9,14] Although the original work by Mars and van Krevelen[15] did not include any atomistic description of the elementary steps, it is nowadays very often associated with the participation of lattice oxygen from the catalyst in the oxidation reaction. Here, we will use the term lattice oxygen for oxygen atoms that induce oxygen vacancies in the metal oxide catalyst upon their removal, as suggested by Morrison,[16] though the discrimination

from adsorbed oxygen is not always straightforward. Within the MvK mechanism, that is better to be called redox mechanism, the catalyst has to fulfill several functions. First, the catayst surface has to provide binding sites for the substrate and intermediates. Second, the catalyst has to be able to exchange oxygen with the gas phase, since the catalyst, or more precisely the active site, has to adsorb molecular oxygen and convert (reduce) it to an active form that is able to oxidize the alkane. For this (oxygen) reduction process the catalyst has to provide electrons. Eventually, the electrons have to be transferred back to the catalyst before the oxidation product can desorb into the gas phase. Consequently, the third prerequisite for an oxidation catalyst is the ability for electron exchange, whereupon one site could in principle manage all three functions. Redox exchange capability (i.e. electron exchange) and exchange of surface "lattice" oxygen should be prerequisites for selective oxidation catalysts (as defined within the MvK concept). Experimental evidence has been often based on analyses probing the boundary case of a "stoichiometric" reaction of the catalyst with either oxygen or the alkane,[4,14,17,18] or under unusual reaction conditions (e.g. pulse mode, vacuum).[8,19] However, such experiments do not necessarily describe the mode of operation under "normal" reaction conditions (except for the riser reactor), where both oxygen and the substrate are present, probably defining a different chemical and electronic surface structure (and working mode) of the catalyst.[20]

Recently, the microwave cavity perturbation technique (MCPT) was introduced to the field of catalysis as noncontact alternative to conventional 2-contact conductivity measurements for probing charge transfer and redox properties of catalysts.[21–23] The contactless and integral nature of this method allows the reaction being performed in a conventional fixed-bed flow-through reactor with a powder catalyst under high-performance catalytic, i.e. nearly technical conditions, while deducing electrical and dielectric materials properties. In this contribution, we applied MCPT to determine the complex permittivity and conductivity of different representative vanadium (III), (IV) and (V) phosphorus oxides under n-butane oxidation conditions: $V^{III}PO_4$, $(V^{IV}O)_2P_2O_7$, $Ag_6(V^{IV}O)_2(PO_4)_2(P_2O_7)$, $Ag_2V^{IV,V}P_{1.6}O_{7+\delta}$, $Ag(V^{IV}O)(V^{V}O)(PO_4)_2$, β-$V^{V}OPO_4$, and α-$V^{V}O$-PO_4. The aim of this study was to validate the two pillars of selective oxidation catalysis,[24] lattice

oxygen exchange and redox behavior, and to identify electronic properties that are characteristic for selective n-butane oxidation catalysts. By measuring the microwave conductivity at different chemical potentials of oxygen and n-butane, the nature of band bending and hence the majority charge carrier type was identified for each sample. Here, the conductivity was also measured under the extreme cases of strongly oxidizing (alkane-free) and reducing (oxygen-free) conditions, respectively. However, the oxidized and reduced ("extreme") states could be directly compared to the electronic state of the working catalyst under normal reaction conditions, and correlated with the catalytic properties of the studied samples. In particular, the reversibility and the kinetics of the observed redox processes were studied, thus defining physical descriptors for selective catalysts that go beyond the simple terms redox and oxygen exchange capability. As for the established catalyst VPP, these results were rationalized by complementary analytical techniques such as in situ near-edge X-ray absorption fine structure spectroscopy (NEXAFS), in situ Raman spectroscopy and temperature-programmed oxidation/reduction (TPO/R).

Results and Discussion

As benchmark catalyst vanadyl pyrophosphate was investigated. A technical sample provided by BASF SE was studied by in situ MCPT, in situ NEXAFS, in situ Raman spectroscopy and TPO/R in order to validate its structural and electronic properties. It is to note, that MA, CO and CO_2 were the only products found in the oxidation of n-butane with VPP. Figure 1a shows the microwave conductivity and real part of the permittivity ε_1 of VPP starting with a gas mixture containing 1.4% n-butane and 20% O_2, which was followed by an oxygen-lean mixture (10% O_2, 1.4% n-butane). While the simultaneously measured n-butane conversion drops from 32 to 26%, the selectivity to MA increases only slightly from 74 to 76% upon changing from the alkane-lean to the oxygen-lean gas phase (Figure 1b). As for the conductivity, only a very small, hardly discernable decrease from 4.3 to 4.1x10^{-5} S cm^{-1} is observed between these two conditions. Furthermore, a strongly oxidizing atmosphere containing 20% O_2 in N_2 has a severe impact on the VPP conductivity,

inducing an increase to 6.7x10^{-5} S cm^{-1} within one hour. The subsequent treatment in a reducing atmosphere of 1.4% n-butane in N_2 does inititially reverse this behavior, i.e. the conductivity falls back to 4.0x10^{-5} S cm^{-1}. However, this is followed by an increase to 6.0x10^{-5} S cm^{-1}. The final treatment in the lean reaction gas mixture discloses a fully reversible behavior of the electronic properties of the catalyst, i.e. it shows nearly the same conductivity as observed at the beginning of the measurement. As for the catalytic properties, the conversion and MA selectivity is with 30 and 74%, respectively, in a similar range as observed in the first cycle under lean reaction conditions, aside from a slight deactivation of the activity from 35 to 30% n-butane conversion over the whole measurement time. Notably, the real part of the permittivity ε_1 is rather constant over the whole measurement range irrespective of gas atmosphere, exhibiting values between 11 and 12, the small variations being within the measurement error. This suggests that the lattice of the bulk catalyst remains stable upon the different treatments and that the conductivity changes (due to bound and/or free charge carriers) are not due to bulk phase transformations. Notably, no changes in the X-ray powder diffractogram and lattice parameters of VPP have been observed under oxidizing or reducing conditions (Supplementary Table S1), which is further evidence for the stability of the bulk phase under all conditions applied.

The measured conductivity values are on the upper limit of the VPP conductivity measured with AC contact methods, usually ranging between 10^{-5} and 10^{-9} S cm^{-1} under similar conditions.[25–29] However, such comparisons are not straightforward due to the strong frequency dependence of the conductivity, if a charge carrier hopping mechanism has to be considered,[30] as has been suggested for V_2O_5.[31]

The conductivity increase in oxidizing and decrease in reducing gases (except for the subsequent rise after longer reducing times, that will be explained later) can be described best by a p-type semiconductor band model[16,32] and is in perfect agreement with the behavior observed by contact methods.[25,26,28,33] The dynamic conductivity was explained by the exchange of lattice oxygen (O_O^x), the associated formation/filling of oxygen vacancies ($V_O^{\bullet\bullet}$), and the coupled generation/depletion of electron holes ($h^\bullet$) being the majority charge carriers (in Kröger-Vink notation,[32]

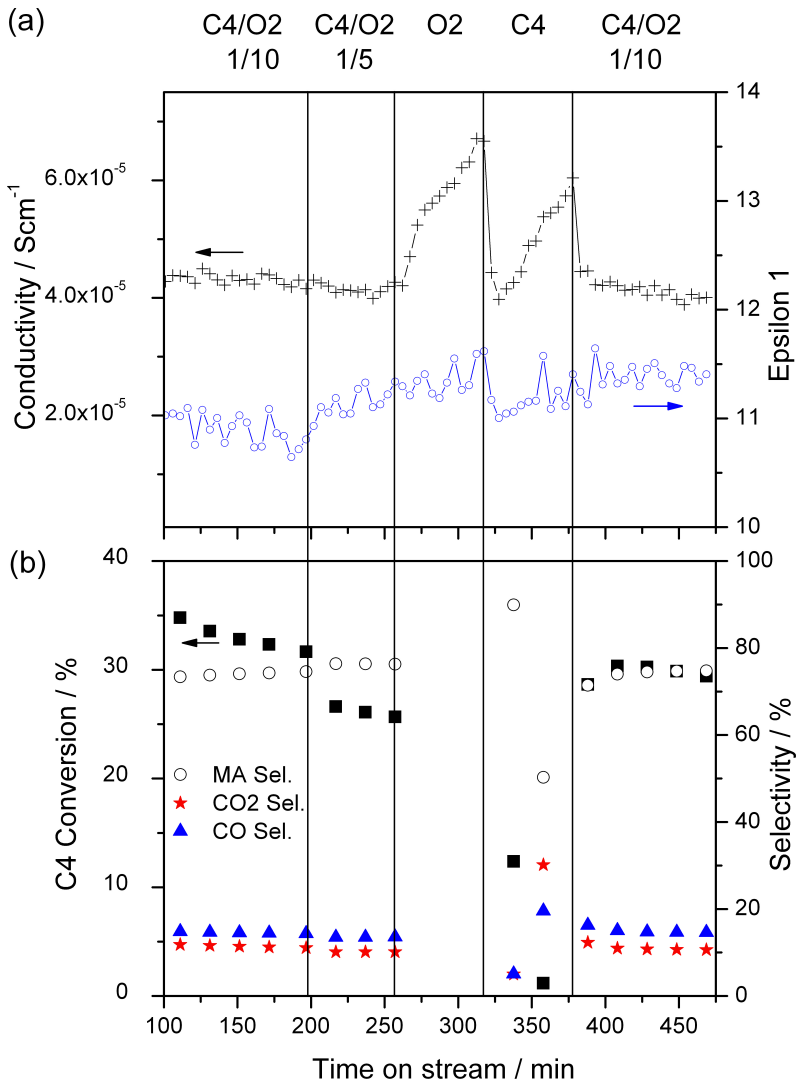

Figure 1: Microwave conductivity, real part of the permittivity ε_1 (a), and catalytic performance (b) of VPP in different gas atmospheres at 385 °C, GHSV = 4240 cm^{-1}. Gas mixtures: C4/O2 (1/10): 1.4% n-C_4H_{10}, 20% O_2; C4/O2 (1/5): 1.4% n-C_4H_{10}, 10% O_2; O2: 20% O_2; C4: 1.4% n-C_4H_{10}; residual gas always N_2.

assuming that all involved oxygen atoms and charge carriers are supplied by the catalyst):

$$^1/_2O_{2\,(g)} + V_O^{\bullet\bullet} \rightarrow O_O^x + 2h^\bullet \quad (1)$$

$$C_4H_{10} + 7O_O^x + 14h^\bullet \rightarrow C_4H_2O_3 + 4H_2O + 7V_O^{\bullet\bullet} \quad (2)$$

In addition, the results of the in situ V L_3 edge NEXAFS measurements with the same catalyst under comparable reaction conditions are depicted in Figure 2a, whereas the simultaneously measured MA production rate (detected by proton-transfer reaction mass spectrometry, PTR-MS) is displayed in Figure 2b, proving that the catalyst was indeed working despite the reduced pressure conditions (total reaction cell pressure: 0.5 mbar). It has been shown that the overall peak position at the V L_3 absorption edge is related to the formal oxidation state of vanadium (the higher the first momentum E_{center}, the higher the oxidation state),[34] and thus can be used to compare V oxidation states of the catalyst in different atmospheres. The first momenta of the V L_3 edge spectra ($E_{\text{center}} = \int E * TEY(E) dE$; with TEY being the total electron yield) in different gas mixtures are plotted in Figure 2c. As a result, the oxidation state is highest under oxidizing, and lowest under reducing conditions, whereas intermediate values of the first momentum are obtained in alkane-lean and richer reaction conditions, at which the differences between the latter conditions are rather small. This is in good agreement with the in situ X-ray photoelectron spectroscopy (XPS) results of VPP published earlier,[23] disclosing a gas phase dependent average surface V oxidation state between 4.0 and 4.3 (measured at a photoelectron kinetic energy of 160 eV and corresponding to an information depth of 1 nm), and resembles the dynamic microwave conductivity behavior shown before. NEXAFS in the total electron yield mode is generally more bulk sensitive than XPS. The 1st momentum of the V L_3 edge spectrum changes at most by 0.16 eV (between condition "O2" and "C4"), which corresponds in a first approximation[34] to a change of the oxidation state by 0.1-0.2 (e.g. from 4.0 to 4.1-4.2). This would be in agreement with the evaluation of the V$2p_{3/2}$ XPS spectrum measured at a photoelectron kinetic energy of 760 eV (corresponding to an information depth of 4 nm) and giving maximum oxidation state changes between 4.0 and 4.15.[23]

This points to a respective information depth for the NEXAFS experiment, that can be expected if Auger electrons contribute primarily to the signal.

These results and the respective conductivity behavior suggest that the concentration of electron hole charge carriers is in equilibrium with the V^{4+}/V^{5+} ratio after

$$(V^{V}O)^{\bullet}_{VO} \rightleftharpoons (V^{IV}O)^{x}_{VO} + h^{\bullet}, \tag{3}$$

and supports the often discussed[16] role of a narrow V 3d band or local V surface states as acceptor band/states giving rise to the p-type conductivity of VPP. However, the pronounced decrease of the vanadium oxidation state in n-butane ("C4") is not reflected in the conductivity response. The difference might be an effect of the different total pressures and thus chemical potentials in the two experiments (n-butane conversion in the NEXAFS experiment is below 1%), or due to the formation of electronically isolated reduced vanadium species on the surface (such as V^{3+}). A third explanation (but closely related to the first argument) is the prevention of a strong reduction of the catalyst due to coke formation under reducing conditions at ambient pressures and high conversions, which will be discussed next.

As described before, it has been found that after the expected sharp initial decline the conductivity was rising again in gas mixtures containing 1.4% n-butane in N_2 (Figure 1a). In order to find an explanation for this unexpected behavior, in situ Raman spectroscopy was performed. In Figure 3 Raman spectra of VPP under reaction, oxidizing, inert, reducing and again oxidizing conditions are shown. During all treatments signatures at 929, 1131 and 1178 cm^{-1} were observed. The first band can be assigned to the pyrophosphate P-O-P stretching vibration, whereas the two latter signals can be attributed to V-O-P stretching bands of VPP.[35–38] A very weak shoulder around 1000 cm^{-1} might be assigned to V=O that could be an indication for a very small concentration of V^{5+} species,[37] probably located mainly on the surface. Besides, no signals to be attributed to alternative vanadium oxide or phosphate bulk phases such as $VOPO_4$[35–38] appeared, proving that the sample consists of phase-pure VPP that is stable in all gas mixtures applied. However, in the

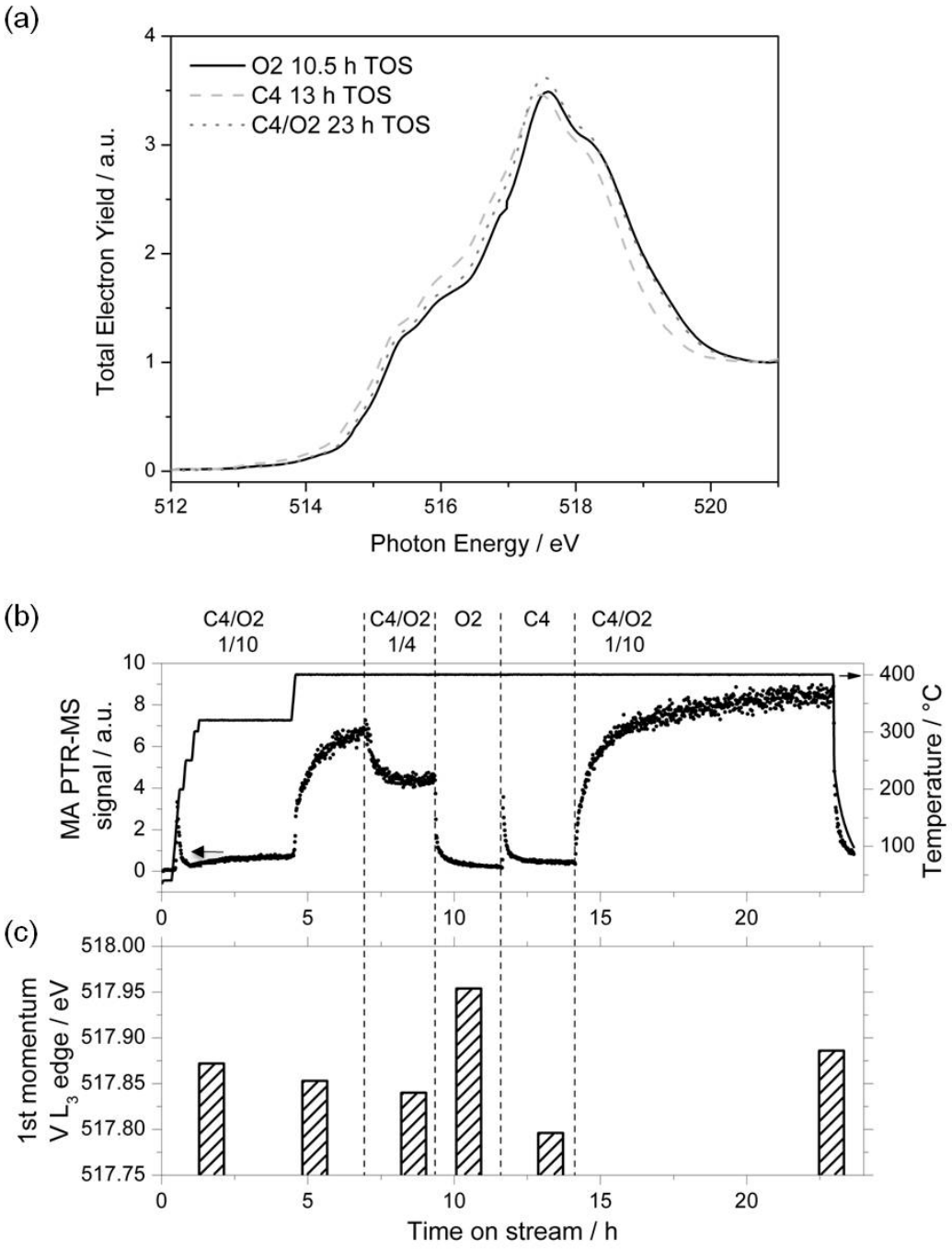

Figure 2: a) In situ V L_3 NEXAFS spectra of VPP in different gas mixtures after the respective time on stream (TOS), b) PTR-MS signal of MA and applied temperature program and c) first momenta of the normalized spectral distributions ($E_{\text{center}} = \int E * \text{TEY}(E) dE$) at the V L_3 edge of VPP in different gas mixtures. Gas mixtures: C4/O2 (1/10): 0.5 sccm *n*-C_4H_{10}, 5.0 sccm O_2; C4/O2 (1/4): 0.5 sccm *n*-C_4H_{10}, 2 sccm O_2, 3 sccm He; O2: 5.0 sccm O_2, 0.5 sccm He; C4: 0.5 sccm *n*-C_4H_{10}, 5.0 sccm He.

reducing mixture containing 2% *n*-butane in He, an additional broad feature at 1580 cm^{-1} showed up with increasing intensity. In this spectral region graphitic carbon shows a specific Raman signal known as G-band.[39] In addition, a very weak and broad signal around 1360 cm^{-1} appeared that can be assigned to the D-band of defective carbon species.[39] Thus, the new Raman signals, evolving under reactive conditions within minutes, can be explained by coke formation on the catalyst. Coking is a very frequently observed phenomenon in alkane oxidation reactions,[38] in particular in strongly reducing environments, and was also reported for VPO catalysts and even given as a principal source for CO and CO_2 by-product formation.[4] As expected, the coke can be removed by introducing an oxidizing gas flow containing 20% O_2 in He. Under such oxidizing conditions the bands at 1360 and 1580 cm^{-1} disappeared, obviously due to an oxidation of the coke to CO_x. Now, the observed microwave conductivity behavior of the sample in Figure 1a can be understood. Graphitic carbon is a rather strong electronic conductor, exceeding the conductivity of VPP by orders of magnitude (10 GHz conductivity of graphite: 0.5-1 Sm^{-1}; carbon black: 0.04-0.2 Sm^{-1}),[40] perfectly explaining the increasing conductivity in the strongly reducing environment.

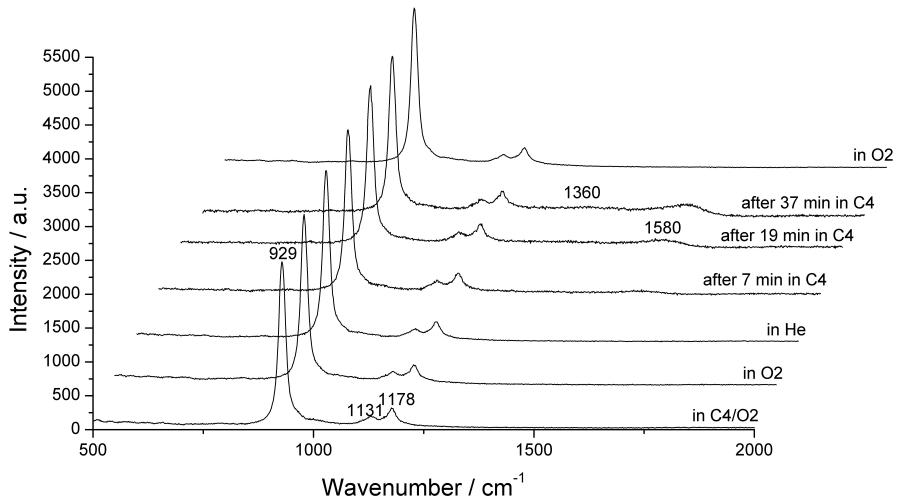

Figure 3: In situ Raman spectra of VPP in different gas atmospheres at 400 °C, initial VPP weight: 80 mg, gas flow: 10 ml/min. C4/O2: 2% *n*-C_4H_{10}, 20% O_2; O2: 20% O_2; C4: 2% *n*-C_4H_{10}; He: 100% He; residual gas always He.

The amount of exchangeable oxygen in VPP between room temperature and 450°C was quan-

tified by temperature-programmed oxidation (TPO1 in Figure 4) in 5% O_2 in He, succeeded by temperature-programmed reduction (TPR1) in 5% H_2 in Ar. This oxidation/reduction cycle was repeated (TPO2 and TPR2, respectively). From the integrals of the measured absolute consumption of O_2 and H_2, respectively, the relative amount of exchanged oxygen of VPP was calculated and plotted versus temperature (Figure 4). As for TPO, at 385°C the determined amount of consumed oxygen would correspond to 0.22% of VPP lattice oxygen. The TPR experiment revealed that the consumption of hydrogen up to 385°C would correspond to the extraction of 0.15% of VPP lattice oxygen. For both TPO and TPR a relative total oxygen exchange of 0.35% was obtained at 450°C. These results show, that 1) the as-received catalyst (run under lean reaction conditions for more than 100 hours) is in a reduced state, and that 2) the redox processes are at least within one redox cycle reversible. The differences between the TPO and TPR curves below 450°C might be due to the different kinetics of the reduction and oxidation processes. While both TPR measurements show within the measurement error no differences and hence indicate the reversibility of the oxygen exchange, the second TPO curve is shifted to lower temperatures and results in a higher absolute O_2 consumption. An explanation could be the formation of OH^- and H_2O and/or the irreversible formation of small amounts of thermodynamically very stable vanadium(V) phases (not yet observable with Raman or XRPD), that might also give rise to the slight but constant decrease of the cataytic activity and conductivity (cf. Figure 1). In contrast, the reversible TPR cycles likely reflect only the reversible exchange of oxygen on the surface.

One of the strongest XRPD signals of VPP can be found at 2θ=23.0° (Supplementary Figure S1), that are assigned to {200}-plane reflections. This might suggest that {100} cleavage planes are dominating the surface, which are also discussed as active layers for MA formation.[17,25] The density of V atoms on this plane is about 8.3 μmol/m^2 according to the determined unit cell parameters (Supplementary Table S1). This would correspond to a theoretical surface oxygen capacity of 66 μg/m^2, assuming a V^{4+}/V^{5+} redox couple. With a BET surface area of 24 m^2/g a surface oxygen capacity of 159 μg per 100 mg catalyst is obtained. Accordingly, 0.22% of exchangeable oxygen determined at 385°C would correspond to 103 μg/100 mg catalyst, complying

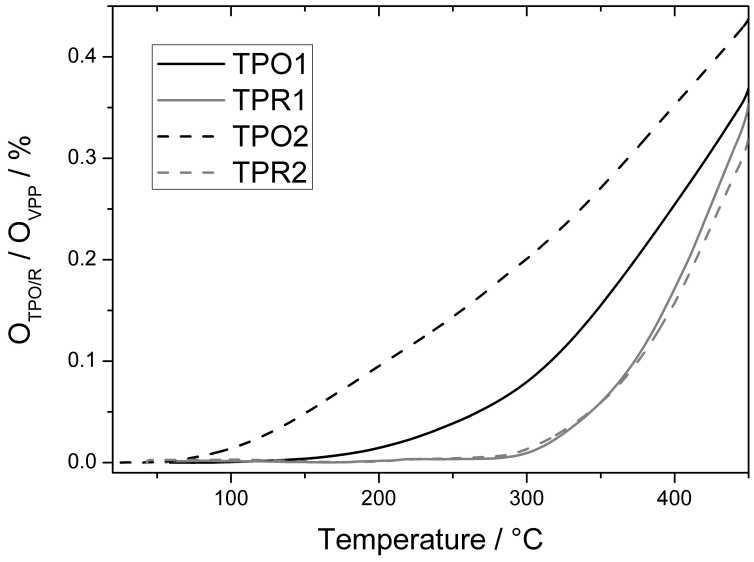

Figure 4: Temperature-programmed oxidation (TPO) and reduction (TPR) plots of VPP in integral units of the relative amount of inserted (TPO) and extracted (TPR) VPP lattice oxygen, respectively.

with 65% of the theoretical total surface oxygen capacity. At 450°C, 164 µg/100 mg lattice oxygen was exchanged, which is close to the theoretical maximum surface capacity. These data suggest that the reversible oxygen exchange mainly involves the catalyst surface. This result fits nicely to the observed surface restriction of the vanadium oxidation state change proven by NEXAFS and XPS, the stability of the bulk phase shown by XRD and Raman spectroscopy, and points to the surface sensitivity of the measured microwave conductivity of the sample depending on the applied gas phase chemical potentials.

Having identified the electronic properties of the benchmark catalyst VPP, its gas-sensitive electronic behavior is to be compared to other selective, inselective or inactive vanadium phosphates. For this purpose, the microwave conductivity and permittivity of the inselective samples $V^{III}PO_4$, α-$V^{V}OPO_4$ and β-$V^{V}OPO_4$ (crystal structures shown in Figure 5) was measured (Figure 6a). It is to note, that α_I- or α_{II}-$VOPO_4$ are spectroscopically hardly descernible from the $VOPO_4 \cdot 2H_2O$ phase. Moreover, the layered α-$VOPO_4$ structure (Figure 5d,e), which is most

likely present at the high reaction temperatures, intercalates easily water between the layers and transforms reversibly into the dihydrate at lower temperatures.

There are only very few catalysts known exhibiting reproducible, stable and at least moderate selectivities to MA. Recently, Karpov et al. identified a sample with the empirical formula $Ag_2V^{IV,V}P_{1.6}O_{7+\delta}$ ($0<\delta<0.5$), supposedly having a vanadyl (IV,V) orthophosphate-pyrophosphate layer structure, since its XRPD pattern (Supplementary Figure S2) resembles the recently characterized $Ag_6(V^{IV}O)(PO_4)(P_2O_7)$ structure (Figure 5b).[41] The former sample exhibited promising selectivities to MA, and thus was included as selective catalyst in our study. For comparison, the phase-pure samples $Ag_6(V^{IV}O)(PO_4)(P_2O_7)$ and $Ag(V^{IV}O)(V^{V}O)(PO_4)_2$, the latter originally synthesized and characterized by Raveau et al.,[42] were tested as well (Figure 6a). All samples were investigated by the same protocol under isothermal conditions at 385°C and a GHSV of 4240 h^{-1} (i.e. contact time: 0.85 s): after 2 hours in the lean reaction gas mixture containing 1.4% n-butane and 20% O_2, the samples were exposed for two hours to an oxidizing mixture (20% O_2 in N_2), followed by a one-hour inert treament in N_2. Then, the gas mixture was switched back for one hour to lean reaction conditions, followed by a strongly reducing atmosphere containing 1.4% n-butane in N_2 for one hour. As for the VPP sample, the latter treatment was restricted to 30 minutes. Instead, VPP was exposed subsequently to 20% O_2 and to a final treatment in 2% H_2 in N_2. The latter conditions were applied to verify the p-type conductivity behavior of VPP in reducing atmospheres excluding the effect of coking. As a result, the conductivity behavior of VPP is in perfect agreement with the aforementioned description within the p-type semiconductor model. The initial decrease upon the second treatment in O_2, followed by a steady increase can be well explained by the removal of coke (diminishing initially the conductivity), as already observed by Raman spectroscopy (Figure 3), and the subsequent increase due to the oxidation of the catalyst surface, which is as expected for a p-type semiconductor. In H_2 the conductivity drops immediately to the level already observed under lean reaction conditions. The latter observation is further evidence for coking being responsible for the originally unexpected conductivity behavior under n-butane-rich conditions.

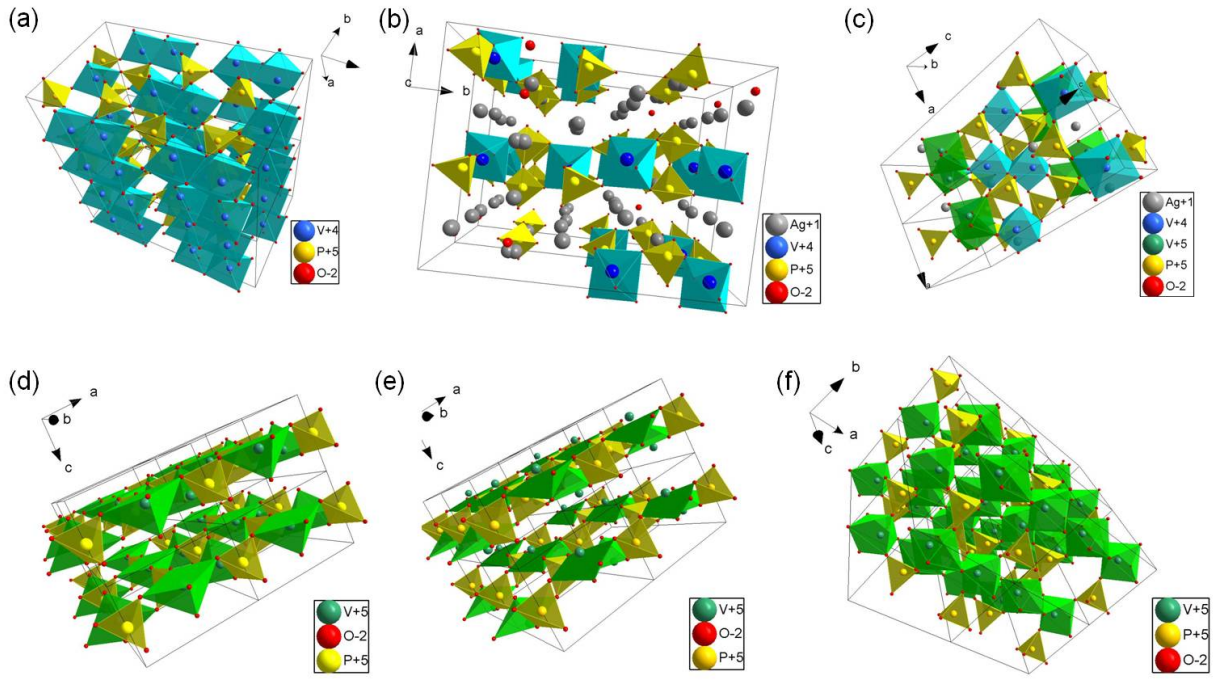

Figure 5: Images of the crystal structures of a) $(V^{IV}O)_2P_2O_7$, b) $Ag_6(V^{IV}O)(PO_4)(P_2O_7)$, c) $Ag(V^{IV}O)(V^{V}O)(PO_4)_2$, d) α_I-$V^{V}OPO_4$, e) α_{II}-$V^{V}OPO_4$, f) β-$V^{V}OPO_4$.

The catalytic properties, conductivities and permittivities of all samples measured in different gas atmospheres are depicted in Figure 6 and are summarized for the lean reaction condition ("C4/O2") in Table 1. Notably, for all active samples CO and CO_2 were the only products observed in significant amounts (besides MA when indicated). Moreover, it is obvious that none of the investigated materials come even close to the MA yield obtained with VPP. Only the novel sample $Ag_2V^{IV,V}P_{1.6}O_{7+\delta}$ shows a moderate and stable MA selectivity of 25%, while the n-butane conversion is with 2.5% rather low (but stable). At higher temperatures (430°C) the selectivity was decreasing to 13% at a conversion of 24%, as was shown in an earlier study (with a GHSV of 2000 h^{-1}).[41] Interestingly, the monovalent silver vanadyl (IV) orthophosphate-pyrophosphate $Ag_6(V^{IV}O)(PO_4)(P_2O_7)$ shows no MA selectivity at all, despite its structural similarities to $Ag_2V^{IV,V}P_{1.6}O_{7+\delta}$. Its activity is with a conversion of 0.4 to 0.8% very low. In contrast, the mixed vanadyl (IV,V) silver orthophosphate and β-$VOPO_4$ produce MA, though with a low selectivity of 10-15% and an n-butane conversion of about 1%. The low but reproducible conversions allow the investigation of the catalysts under nearly differential conditions, hence avoiding steep

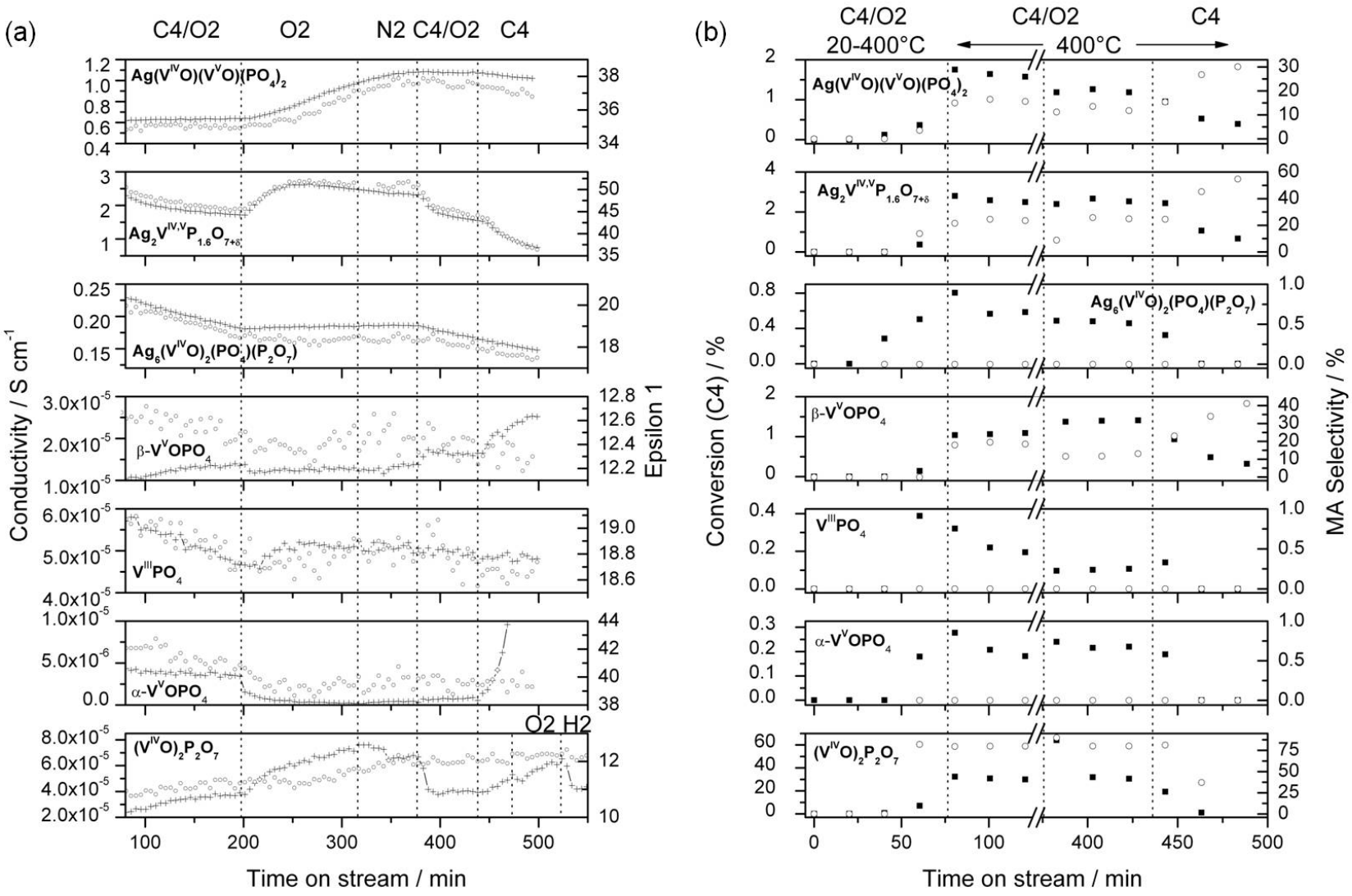

Figure 6: a) Microwave conductivity (crosses), real part of the permittivity ε_1 (open circles), and b) *n*-butane conversion (squares) and MA selectivity (open circles) of selected vanadium phosphates in different gas atmospheres at 385 °C, GHSV = 4240 cm^{-1}. Gas mixtures: C4/O2: 1.4% *n*-C_4H_{10}, 20% O_2; O2: 20% O_2; N2: 100% N_2; C4: 1.4% *n*-C_4H_{10}; H2: 2.0% H_2; residual gas always N_2.

concentration and conductivity gradients in the fixed bed. This is an advantage in light of the integral nature of MCPT measuring the overall conductivity of the sample, which is to be correlated with the chemical potential of the gas phase (that is only known upstream and downstream of the catalyst). The other samples VPO_4 and α-$VOPO_4$ can be regarded as inactive (and unselective), since only minor amounts of CO_x are produced.

Table 1: Catalytic activities, selectivities and microwave conductivities of the different vanadium phosphate samples measured at the end of the second cycle under reaction conditions (cf. Figure 6): T=385°C, GHSV=4240 h^{-1} (5 ml/min); gas mixture: 1.4% n-butane, 20% O_2, residual gas N_2.

Sample	$X_{n\text{-butane}}$ [%]	S_{MA} [%]	S_{COx} [%] CO_2+CO	$Rate_{MA}$ [mol/(m^2min)]	σ [Scm^{-1}]	Cond. type
$(V^{IV}O)_2P_2O_7$	31	80	10+10	$4.6x10^{-7}$	$4.0x10^{-5}$	p
$Ag_6(V^{IV}O)_2(PO_4)(P_2O_7)$	0.5	0	100+0	0	0.17	p
$Ag_2V^{IV,V}P_{1.6}O_{7+\delta}$	2.5	25	38+37	$2.7x10^{-8}$	1.6	p
$Ag(V^{IV}O)(V^{V}O)(PO_4)_2$	1.2	12	35+53	$6.1x10^{-9}$	1.1	p
α-$V^{V}OPO_4$	(0.2)	0	(58+42)	0	$9.0x10^{-7}$	n
β-$V^{V}OPO_4$	1.4	13	46+41	$4.3x10^{-8}$	$1.6x10^{-5}$	n
$V^{III}PO_4$	0.1	0	100+0	0	$5.0x10^{-5}$	-

It is now interesting to compare the simultaneously measured (dynamic) conductivity and permittivities under the respective conditions (Figure 6a). First, all vanadyl (IV) catalysts, including the mixed vanadyl (IV,V) phosphates, show an increasing conductivity in O_2 and a decreasing conductivity in the n-butane atmosphere. As described before, this can be interpreted in terms of a p-type semiconducting behavior. Although $Ag_6(V^{IV}O)(PO_4)(P_2O_7)$ is obviously unstable in the presence of n-butane (or more likely its surface) exhibiting a constantly falling conductivity, it is stabilized in inert or oxidizing conditions, thus justifying its classification as p-type semiconductor. In contrast, the conductivities of the two vanadyl (V) orthophosphates show the opposite trend, a decreasing value under oxidizing and a rising conductivity under reducing (or reaction) conditions. Hence this can be explained by electrons being the majority charge carriers, classifying these sam-

ples as n-type semiconductors. The p-type and n-type conductivity of VPP and the two $VOPO_4$ samples, respectively, is in agreement with contact measurements at low frequencies.[26] The other materials have not been measured by DC or AC methods yet.

Interestingly, the conductivity of VPO_4 remains basically constant and does not respond systematically to the different gas mixtures. Hence it can be summarized that the investigated compounds with a bulk vanadium oxidation state of +4 (or mixed +4/+5) exhibit p-type, samples with an oxidation state of +5 show n-type semiconductivity, while the V^{3+} phosphate does not react on the gas atmosphere.

Another important result is that the conductivity of the silver vanadyl phosphates is orders of magnitudes higher than for the other samples. In general, Ag^+ ions in the different crystal layer structures are located between the layers (Figure 5). Hence charges might be transferred easily between the Ag ions forming a delocalized partially filled conduction band, giving rise to the high conductivity due to the high number of charge carriers and/or very high mobilities. Ionic conductivity of Ag^+ might be another explanation, though in general the high microwave frequency excitation privileges highly mobile electronic compared to inertial ionic charge carriers. However, the characteristic conductivity behavior of the three different silver vanadyl phosphates upon changing the gas phase is probably still governed by the vanadium, since the dynamic behavior resembles the situation found for the silver-free samples, in particular with respect to the vanadium oxidation state.

Moreover, the differences in the gas-phase response of the permittivity ε_1 are striking. Whereas no significant changes are observed for the silver-free samples, the permittivity follows nearly exactly the conductivity trend for the silver vanadyl phosphates (Figure 6a). The real part of the permittivity depends on the polarizability (i.e. electric dipole character) of the material. Thus it is conceivable that large changes of the absolute number or mobility of charge carriers (indicated by the conductivity), as observed in the silver samples upon changing the gas atmosphere, will induce appropriate changes in the dipolar character (polarizability) of the sample. However, this interpretation has to be taken with care, since the resonance frequency shift of the microwave

cavity induced by the sample becomes dependent on the conductivity σ (or the imaginary part of the permittivitiy ε_2) for large conductivities in the vicinity of the depolarization peak,[43] and not only on ε_1 as assumed in our calculation. The exact relationships have to be determined by temperature-dependent measurements of the complex permittivity in the future.

In order to better compare the conductivity kinetic trends of the different samples, the conductivities were normalized to (i.e. devided by) the respective value measured under lean reaction conditions after 190 hours time on stream for each sample. This way, all data could be plotted in one graph (Figure 7). Since the conductivity σ is the product of the charge carrier density N and the mobility μ,

$$\sigma = eN\mu, \tag{4}$$

and under the assumption that the charge carrier mobilities do not depend on the external gas phase, the thus normalized conductivity would allow the direct comparison of the relative changes of charge carrier concentrations in dependence on the gas mixture. Although this hypothesis has to be proven in the future by measuring the mobilities, the general differences between the samples can be already deduced. First, it is remarkable that only the selective samples VPP and $Ag_2V^{IV,V}P_{1.6}O_{7+\delta}$ show a similar behavior, i.e. a strong and fast response to the O_2 atmosphere *and* a stable and reproducible conductivity under reaction conditions, irrespective of the previous treatment. Under oxidative conditions the value for VPP doubles, whereas the conductivity of $Ag_2V^{IV,V}P_{1.6}O_{7+\delta}$ increases by a factor of 1.5. The abrupt change of the conductivity of VPP under inert conditions might be due to the removal of weakly chemisorbed oxygen. Although the unselective sample $Ag(V^{IV}O)(V^{V}O)(PO_4)_2$ exhibits a similarily increasing conductivity in O_2, its slope is much smaller and, even more important, the conductivity stays at the high value under the subsequently applied reaction conditions. A similar, though reversed, behavior is observed for the inactive α-$V^{V}OPO_4$. Here, the conductivity shows a strong and steep decrease in O_2, that does not recover in the reaction gas mixture. Contrarily, the slightly active β-$V^{V}OPO_4$ does recover, but the conductivity difference between oxidizing and reaction gas atmosphere is much smaller

than for the other active samples. As for $Ag_6(V^{IV}O)(PO_4)(P_2O_7)$ and VPO_4, the conductiviy is not stable under reaction conditions or does not respond at all on the gas phase, respectively. In conclusion, a strong reversible response in the sequence C4/O2, O2, C4/O2 might be an indication for the activity and selectivity of the catalyst.

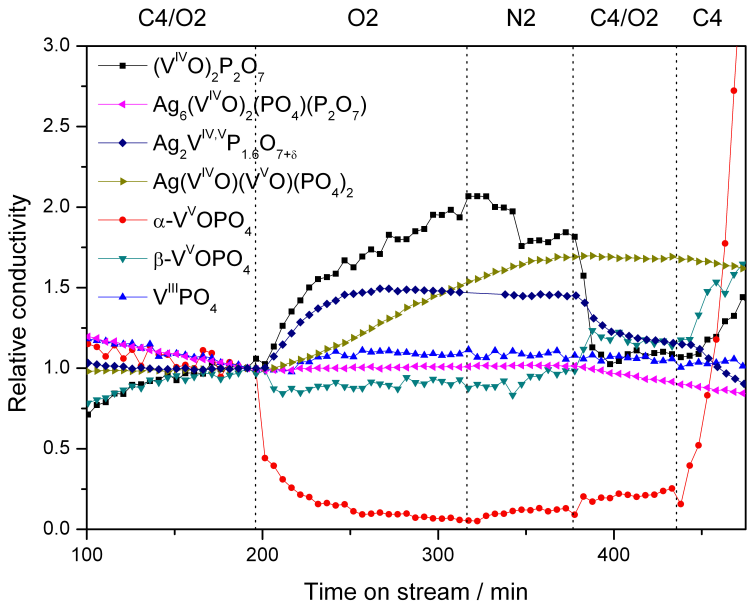

Figure 7: Normalized microwave conductivity of selected vanadium phosphates in different gas atmospheres at 385 °C, GHSV = 4240 cm^{-1}. Gas mixtures: C4/O2: 1.4% n-C_4H_{10}, 20% O_2; O2: 20% O_2; N2: 100% N_2; C4: 1.4% n-C_4H_{10}; residual gas always N_2.

In addition to the reversibility of the conductivity, the behavior under reducing conditions is unique for VPP. Neither in n-butane (where coking disturbs the measurement), nor in H_2 does the conductivity undercut the values observed under reaction conditions. In contrast, the conductivity of the p-type conductor $Ag_2V^{IV,V}P_{1.6}O_{7+\delta}$ is further decreased, whereas the n-type conductors α-V^VOPO_4 and β-V^VOPO_4 exhibit a pronounced increase. Interestingly, $Ag(V^{IV}O)(V^VO)(PO_4)_2$ shows even under strongly reducing conditions only a very slowly falling conductivity.

Moreover, it is remarkable that all vanadium (IV) (and (IV,V)) samples are p-type semiconductors, whereas all vanadium (V) phases are n-type semiconductors. As already indicated by equation (3), in vanadium (IV) oxides a small amount of V^{5+} is needed for the generation of

electron holes. It has been suggested[28] that these electron holes are trapped by lattice oxygen:

$$O_O^x + h^\bullet \rightarrow O_O^\bullet \tag{5}$$

Hence the conductivity could be described as hopping process where the electron hole is transferred between adjacent O^- and O^{2-} ions or within the valence band (exhibiting a strong O character[44,45]).

In vanadium (V) oxides or phosphates, local V^{4+} states or a narrow partially filled V 3d band within the band gap have been suggested,[16] and were indeed identified in V_2O_5 single crystals.[45] These states can donate electrons into the conduction band and thus explain the n-type semiconductivity of the vanadium (V) samples.

In a next step, we tried to summarize these results exemplarily for the two selective catalysts VPP and $Ag_2V^{IV,V}P_{1.6}O_{7+\delta}$ in schematic band diagrams (Figure 8). Due to the gas phase sensitivity of the measurements and the finding, that only the surface participates in the reaction (as proven for VPP), the samples are best described as solid-state gas sensors (chemiresistor).[16,46] Then, the V^{4+}/V^{5+} redox couple can be identified as surface state exchanging electrons with the gas phase (adsorbed molecules). The emptied surface state would correspond to V^{5+}, the occupied surface state to V^{4+}. This charge transfer will induce a band bending and the formation of a space charge region due to the pinning of the Fermi level to the surface state level (and/or the redox potential of the adsorbed reaction gas). As a consequence, the band bending, which is accompanied by changes in the subsurface charge carrier concentration to screen the surface charge, will control the conductivity in the subsurface region, as was oberved in our MCPT measurements. From this representation it becomes also clear, why vanadium (III) phosphates cannot activate n-butane. The (empty) V^{3+}/V^{4+} surface state lies most probably in any cases above the redox potential of n-butane, thus providing no driving force for the exchange of charge carriers.

This way, the conductivity behavior of the p-type semiconductor $Ag_2V^{IV,V}P_{1.6}O_{7+\delta}$ can be easily understood, with a high conductivity in O_2, an intermediate conductivity in C4/O2, and a low conductivity in C4 (Figure 8a; cf. Figures 6 and 7). This is in contrast to VPP, where the

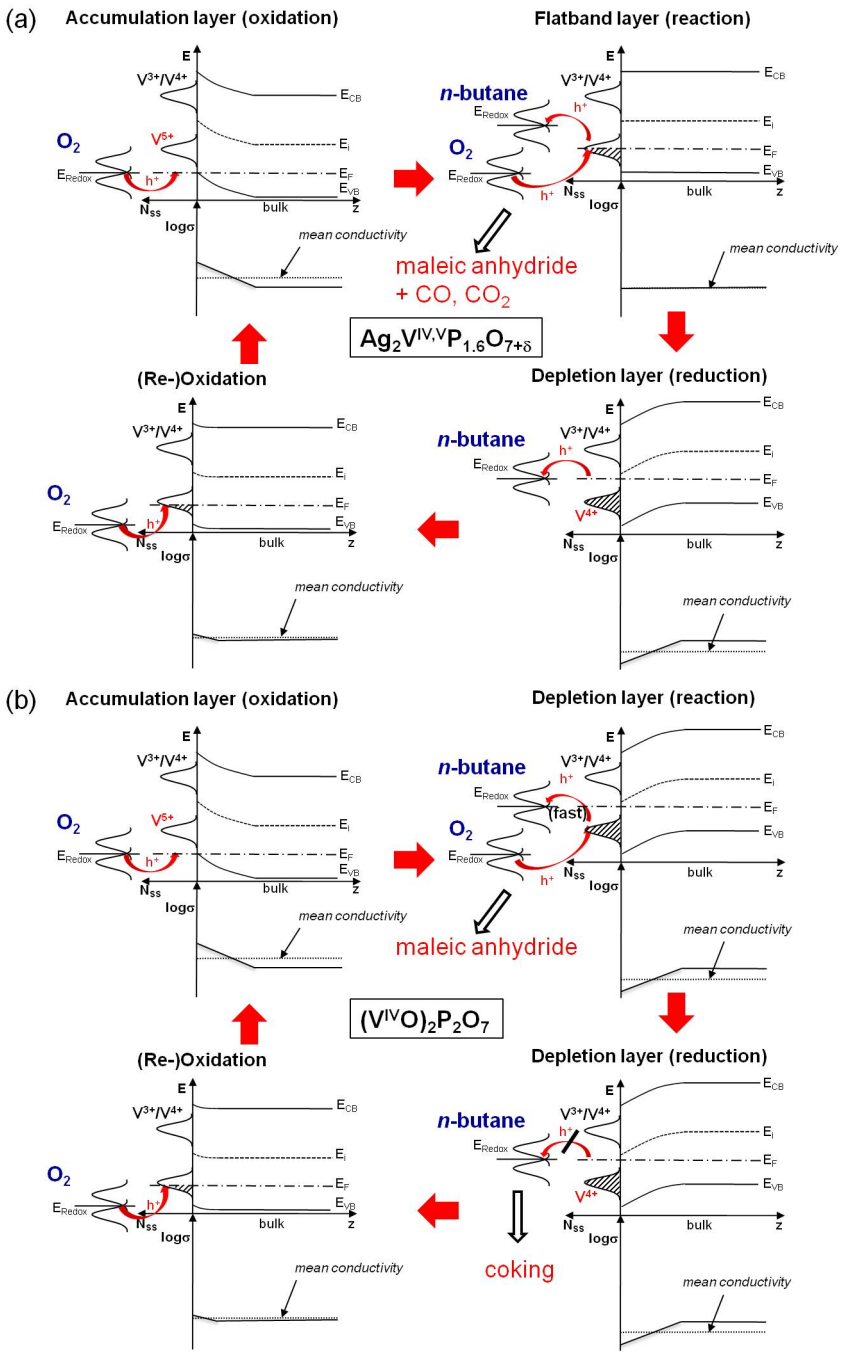

Figure 8: p-Type semiconductor band diagrams with upward band bending upon adsorption of the acceptor molecule O_2 and downward bending upon adsorption of the donor *n* -butane to a V^{4+}/V^{5+} surface state, explaining the different conductivity response of $Ag_2VP_{1.6}O_{7+\delta}$ (a) and VPP (b). E_F: Fermi energy, E_i: intrinsic energy, E_{CB}: conduction band edge, E_{VB}: valence band edge. The arrows indicate the transfer of electron holes due to adsorption of molecules with suitable frontier orbitals and redox energies E_{Redox} at surface states. Additionally, the corresponding local and mean conductivities (as measured by integral methods such as MCPT) of the semiconductors are shown schematically.

conductivity never went below the value already measured in the reaction gas mixture. Here, VPP is already in a strongly reduced state (probably with strong downward band bending, Figure 8b). The absence of oxygen only leads to the formation of coke and not to the formation of oxygenates due to the lack of charge carriers and/or active oxygen. This can be explained by a very fast reduction step (oxidation of n-butane), as already indicated in the conductivity response upon changing the atmosphere to more reducing conditions (Figures 6 and 7). In a low conducting (strongly reduced) p-type semiconductor the transport of charge carriers to the surface is limited due to the increasing electrostatic repulsion with the increasing depletion of electron holes (strong downward band bending). This space charge limited charge transfer might prevent the overoxidation of the substrate, thus being an important prerequisite for highly selective oxidation catalysts, and which was only observed in the highly selective VPP, but in none of the other investigated (inselective) samples. Furthermore, the restriction of the (2-dimenisonal) V^{5+} phase to to the surface can be understood as well, since a 3-dimensional oxidation or reduction of the compound would enormously increase the band bending and hence the electrostatic repulsion within the space charge layer, i.e. the system is self-limiting in the segregation of the surface structure.

Conclusions

In this contribution, the microwave conductivity of the vanadium phosphates $V^{III}PO_4$, $(V^{IV}O)_2P_2O_7$, $Ag_6(V^{IV}O)_2(PO_4)_2(P_2O_7)$, $Ag_2V^{IV,V}P_{1.6}O_{7+\delta}$, $Ag(V^{IV}O)(V^{V}O)(PO_4)_2$, β-$V^{V}OPO_4$, and α-$V^{V}OPO_4$ was investigated by the microwave cavity perturbation technique under different reaction conditions and was compared with the simultaneously measured catalytic performance of these samples in the selective oxidation of n-butane to maleic anhydride. It was found that all vanadium (IV) and (IV,V) samples showed p-type, vanadium (V) phosphates n-type semiconductivity, whereas the vanadium (III) phase exhibited no response on the applied reaction gas mixtures.

As for VPP, it could be shown by XRPD and Raman spectroscopy that the bulk is stable during the redox cycles applied. Moreover, TPR/O and in situ NEXAFS experiments indicate that the

redox activity of vanadium and the oxygen exchange is restricted to the surface region of the catalyst. This proves the high sensitivity of MCPT as indicator for the redox stability of catalysts under operation conditions. It is conceivable that MCPT could be developed as a rapid test method for evaluating high-throughput catalytic data without performing a complete structural analysis for pre-determining promising (even multiphase) catalysts.

Moreover, we could identify three general descriptors of selective and active oxidation catalysts: 1) The conductivity (and surface vanadium oxidation state) changes fast and reversibly with the chemical potential of the gas phase, b) the electronic structure (conductivity and vanadium oxidation state) is stable under reaction conditions, and c) the absolute conductivity under reaction conditions should be as low as possible (compared to strongly reducing conditions for p-type or oxidizing conditions for n-type semiconductors). The latter descriptor is interpreted as physical representation of the "site isolation" principle of selective oxidation catalysts since a low amount of active charge carriers should prevent an overoxidation of the substrate. The absolute conductivity and the majority charge carrier type are probably no (simple) descriptors of selective catalysts, since an alternative compound such as the $MoVTeNbO_x$ M1-phase is active and selective in the oxidation of n-butane, but shows in contrast to VPP a rather high and n-type semiconductivity as identified in preliminary in situ MCPT studies.

Experimental Section

Catalyst preparation

The synthesis and characterization of the benchmark catalyst vanadyl pyrophosphate was described previously.[23] Its X-ray powder diffraction pattern is shown in Figure S1 of the Supporting Information. This catalyst exhibited a BET surface area of 24 m^2/g.

$Ag_2V^{IV,V}P_{1.6}O_{7+\delta}$ ($0 \leq \delta \leq 0.5$) was synthesized by the reaction of silver acetate with V_2O_5 and phosphoric acid in water, using citric acid as reducing agent under reflux and constant stirring. The resulting suspension was filtered and the recovered solid washed with water and dried under

vacuum at 90°C. The XRPD pattern of $Ag_2V^{IV,V}P_{1.6}O_{7+\delta}$ (Supplementary Figure S2), in particular of the post mortem sample measured after the whole measurement cycle, shows similarity to those of $Ag_{0.43}V^{IV,V}O(PO_4)\cdot 2H_2O$,[47] $Ag_2(V^VO_2)(PO_4)$,[41,48] and $Ag_6(V^{IV}O)_2(PO_4)_2(P_2O_7)$[49] (Supplementary Figure S4). The sample exhibited a BET surface area of 7 m^2/g.

In a very similar procedure[49] $Ag_6(V^{IV}O)_2(PO_4)_2(P_2O_7)$ was obtained from $AgNO_3$, V_2O_5, $(NH_4)_2HPO_4$ and vanadium as reducing agent. The same temperatures as reported for $Ag(V^{IV}O)(V^VO)(PO_4)_2$ were used. Thus, the mixed pyrophosphate-orthophosphate was obtained as single-phase product (Supplementary Figure S4) with a BET surface area of 0.3 m^2/g.

$Ag(V^{IV}O)(V^VO)(PO_4)_2$ was synthesized according to a slighty modified procedure described in literature[42] by reacting $AgNO_3$, V_2O_5 and $(NH_4)_2HPO_4$ in the molar ratio 1:0.9:2 for 24 h at 380°C in air. After complete evaporation of all volatile species elemental vanadium was added as reducing agent to set the desired composition. After reaction at 550°C (72 h) in a sealed silica tube, silver-vanadyl(IV)-vanadyl(V)-orthophosphate was obtained as brown, microcrystalline single-phase powder (XRPD in Supplementary Figure S3).

α-V^VOPO_4/$V^VOPO_4\cdot 2H_2O$. The dihydrate (Supplementary Figure S5) was synthesized according to literature[50] by refluxing V_2O_5 in conc. H_3PO_4, filtering the precipitate, washing with water and acetone and drying in air. The anhydrous phosphate was obtained by dehydrating the dihydrate under vacuum at 700°C . The anhydrous phosphate is re-hydrated reversibly and rather fast. The sample exhibited a BET surface area of 6 m^2/g.

By heating α-V^VOPO_4 and traces of moisture in a sealed silica ampoule for 7 d at 500°C the α form was transformed to β-$VOPO_4$. By applying a temperature gradient 700→600°C chemical vapor transport of β-$VOPO_4$ becomes possible, with water acting as transport agent.[51] According to its XRPD pattern (Supplementary Figure S6) the β-modification was obtained as single-phase product with a BET surface area of 1 m^2/g.

Vanadium(III)-orthophosphate was obtained in sealed silica tubes by reducing β-$VOPO_4$ with vanadium phosphide VP. $V^{III}PO_4$ was purified and crystallized by chemical vapor transport. Details on synthesis and crystallization are described in literature.[51,52] The XRPD pattern of the

single-phase material is given in Figure S7 (Supporting Information). The BET surface area was <1 m^2/g.

All powder samples were first pelletized, then the pellets were crushed and for the catalytic and MCPT experiments the sieve fraction of 80-200 μm was used.

Characterization

The MCPT setup and the measurement protocol were described in detail previously.[22,23] In short, as resonator a cylindrical X-band TM_{110} silver-plated brass cavity (ZWG Berlin-Adlershof) with a height of 19.5 mm and a diameter of 38.5 mm was used. A quartz tube plug-flow reactor with 4 mm outer and 3 mm inner diameter containing the sample under investigation (powders were filled in with a bed height of 10 mm and embedded within quartz wool) and surrounded by a 10 mm outer diameter double-walled quartz dewar mantle was directly placed in the center of the cavity. The quartz tube reactor was connected upstream to a gas delivery manifold equipped with mass flow controllers (Bronkhorst El-Flow) and downstream to an on line gas chromatograph (Agilent 7890A). Heating of the reactor was performed by preheating a stream of 8 l/min N_2 in a resistive furnace consisting of a Sylvania tungsten series I heater. The cavity was cooled with two water-circuit-cooled copper plates attached to the resonator endplates and additionally heated by heating wires to maintain a constant resonator temperature of 25 °C. The cavity was connected to a vector network analyzer (Agilent PNA-L N5230C-225) in order to record resonance spectra of S11-parameters in reflection mode (reflected power versus frequency) and to determine the resonance frequency and quality factor of the cavity with and without sample. The microwave power attenuation was set to 11 dBm.

In situ near-edge X-ray absorption fine structure spectroscopy (NEXAFS) has been performed at the synchrotron radiation facility BESSY II of the HZB (Helmholtz-Zentrum Berlin) using monochromatic radiation of the ISISS (Innovative Station for In Situ Spectroscopy) beamline as a tuneable X-ray source. High pressure NEXAFS spectra were obtained in the presence of reactive gases at elevated temperature using the high pressure end station designed and constructed at the

Fritz-Haber-Institut. Details of the set-up are described elsewhere.[53] In brief, 5 mg of VPP powder was pressed into a self-supporting disc (5 tons pelletizing pressure, pellet diameter: 8 mm) that was mounted inside a reaction cell onto a sapphire sample holder approximately 1200 μm in front of the 1st aperture of a differentially pumped electrostatic lens system. The home-built electron lens serves as the input system for a (modified) commercial hemispherical electron analyzer (PHOIBOS 150, Specs-GmbH). Gases are introduced to the cell via calibrated mass flow controllers, heating is provided by a NIR laser (808 nm, cw) at the rear of the sample, and the temperature is monitored by a thermocouple attached directly to the sample surface.

As for the in situ Raman experiments the catalyst sample was placed in a temperature-controlled Raman cell (Linkam CCR1000) which is mounted on a microscope stage. 1 mW of an Ar-ion laser (Spectra-Physics Stabilite 2018) operating at 488 nm were focused on the sample and the scattered light was analyzed in a grating spectrometer coupled to a CCD camera (Princeton Instruments, 500 gr/mm, 750 mm).

Temperature-programmed oxidation and reduction experiments were performed in a tube furnace (Carbolite). The catalyst was placed above a frit in a fixed-bed reactor. The temperature was measured with a thermocouple (K-type) in the sample and the O_2/H_2 gas concentration was analyzed by TCD detectors (Rosemount Analytical). The applied temperature ramp was always 6 K/min. Before the measurements the sample was pre-heated in He at 400°C to remove residual water and adsorbates.

Nitrogen adsorption was carried out at 77 K on a Quantachrome Autosorb-6B analyzer to measure the specific surface area. Prior to the measurement, the sample was outgassed in vacuum at 250°C for 3 h. The specific surface area S_{BET} was calculated according to the 11-point Brunauer-Emmett-Teller method (BET) in the p/p_0 = 0.05-0.3 pressure range.

Acknowledgement

The present work has been supported by the German Federal Ministry of Education and Research (BMBF) as part of the ReAlSelOx project, grant number 033R028. The authors thank Dr. Frank

Girgsdies for XRPD and Florian-Fabien Rybicki (both FHI) for BET measurements. The HZB staff is acknowledged for their continual support of the high-pressure electron spectroscopy activities of the FHI at BESSY II. We are very grateful to Prof. R. Stößer (Humboldt-Universität zu Berlin) for his steady support regarding the development of the microwave cavity perturbation technique.

References

(1) Bartholomew, C. H.; Farrauto, R. J. *Fundamentals of industrial catalytic processes*, 2nd ed.; Wiley-Interscience: Hoboken, New Jersey, 2006.

(2) Cavani, F. *Catal. Today* **2010**, *157*, 8–15.

(3) Cavani, F.; Teles, J. H. *ChemSusChem* **2009**, *2*, 508–534.

(4) Pepera, M. A.; Callahan, J. L.; Desmond, M. J.; Milberger, E. C.; Blum, P. R.; Bremer, N. J. *J. Am. Chem. Soc.* **1985**, *107*, 4883–4892.

(5) Centi, G.; Trifiro, F.; Ebner, J. R.; Franchetti, V. M. *Chem. Rev.* **1988**, *88*, 55–80.

(6) Centi, G. *Catal. Today* **1993**, *16*, 5–26.

(7) Hutchings, G. J.; Desmartin-Chomel, A.; Olier, R.; Volta, J. C. *Nature* **1994**, *368*, 41–45.

(8) Rodemerck, U.; Kubias, B.; Zanthoff, H. W.; Baerns, M. *Appl. Catal. A* **1997**, *153*, 203–216.

(9) Chen, B.; Munson, E. J. *J. Am. Chem. Soc.* **2002**, *124*, 1638–1652.

(10) Hävecker, M.; Mayer, R. W.; Knop-Gericke, A.; Bluhm, H.; Kleimenov, E.; Liskowski, A.; Su, D.; Follath, R.; Requejo, F. G.; Ogletree, D. F.; Salmeron, M.; Lopez-Sanchez, J. A.; Bartley, J. K.; Hutchings, G. J.; Schlögl, R. *J. Phys. Chem. B* **2003**, *107*, 4587–4596.

(11) Bluhm, H.; Hävecker, M.; Kleimenov, E.; Knop-Gericke, A.; Liskowski, A.; Schlögl, R.; Su, D. S. *Top. Catal.* **2003**, *23*, 99–107.

(12) Hutchings, G. J. *J. Mater. Chem.* **2004**, *14*, 3385–3395.

(13) Ballarini, N.; Cavani, F.; Cortelli, C.; Ligi, S.; Pierelli, F.; Trifiro, F.; Fumagalli, C.; Mazzoni, G.; Monti, T. *Top. Catal.* **2006**, *38*, 147–156.

(14) Coulston, G. W.; Bare, S. R.; Kung, H.; Birkeland, K.; Bethke, G. K.; Harlow, R.; Herron, N.; Lee, P. L. *Science* **1997**, *275*, 191–193.

(15) Mars, P.; van Krevelen, D. W. *Chem. Eng. Sci. Spec. Suppl.* **1954**, *3*, 41–57.

(16) Morrison, S. R. *The chemical physics of surfaces*; Springer US, 1990.

(17) Wang, D. X.; Kung, H. H.; Barteau, M. A. *Appl. Catal. A* **2000**, *201*, 203–213.

(18) Lorences, M. J.; Patience, G. S.; Diez, F. V.; Coca, J. *Appl. Catal. A* **2004**, *263*, 193–202.

(19) Abon, M.; Bere, K. E.; Delichere, P. *Catal. Today* **1997**, *33*, 15–23.

(20) Schlögl, R.; Knop-Gericke, A.; Hävecker, M.; Wild, U.; Frickel, D.; Ressler, T.; Jentoft, R. E.; Wienold, J.; Mestl, G.; Blume, A.; Timpe, O.; Uchida, I. *Top. Catal.* **2001**, *15*, 219–228.

(21) Moos, R.; Wedemann, M.; Spörl, M.; Reiss, S.; Fischerauer, G. *Top. Catal.* **2009**, *52*, 2035–2040.

(22) Eichelbaum, M.; Stößer, R.; Karpov, A.; Dobner, C.-K.; Rosowski, F.; Trunschke, A.; Schlögl, R. *Phys. Chem. Chem. Phys.* **2012**, *14*, 1302–1312.

(23) Eichelbaum, M.; Hävecker, M.; Heine, C.; Karpov, A.; Dobner, C. K.; Rosowski, F.; Trunschke, A.; Schlögl, R. *Angew. Chem. Int. Ed.* **2012**, *51*, 6246–6250.

(24) Grasselli, R. K. *Top. Catal.* **2002**, *21*, 79–88.

(25) Abon, M.; Herrmann, J. M.; Volta, J. C. *Catal. Today* **2001**, *71*, 121–128.

(26) Rouvet, F.; Herrmann, J. M.; Volta, J. C. *J. Chem. Soc. Faraday Trans.* **1994**, *90*, 1441–1448.

(27) Sartoni, L.; Delimitis, A.; Bartley, J. K.; Burrows, A.; Roussel, H.; Herrmann, J. M.; Volta, J. C.; Kiely, C. J.; Hutchings, G. J. *J. Mater. Chem.* **2006**, *16*, 4348–4360.

(28) Herrmann, J. M.; Vernoux, P.; Bere, K. E.; Abon, M. *J. Catal.* **1997**, *167*, 106–117.

(29) Ait-Lachgar, K.; Tuel, A.; Brun, M.; Herrmann, J. M.; Krafft, J. M.; Martin, J. R.; Volta, J. C.; Abon, M. *J. Catal.* **1998**, *177*, 224–230.

(30) Sinkkonen, J. *Phys. Status Solidi B* **1981**, *103*, 231–237.

(31) Haemers, J.; Baetens, E.; Vennik, J. *Phys. Status Solidi A* **1973**, *20*, 381–386.

(32) Gellings, P. J.; Bouwmeester, H. J. M. *Catal. Today* **2000**, *58*, 1–53.

(33) Herrmann, J. M. *Catal. Today* **2006**, *112*, 73–77.

(34) Hävecker, M.; Knop-Gericke, A.; Mayer, R. W.; Fait, M.; Bluhm, H.; Schlögl, R. *J. Electron Spectrosc. Relat. Phenom.* **2002**, *125*, 79–87.

(35) Ben Abdelouahab, F.; Olier, R.; Guilhaume, N.; Lefebvre, F.; Volta, J. C. *J. Catal.* **1992**, *134*, 151–167.

(36) Xue, Z. Y.; Schrader, G. L. *J. Phys. Chem. B* **1999**, *103*, 9459–9467.

(37) Conte, M.; Budroni, G.; Bartley, J. K.; Taylor, S. H.; Carley, A. F.; Schmidt, A.; Murphy, D. M.; Girgsdies, F.; Ressler, T.; Schlögl, R.; Hutchings, G. J. *Science* **2006**, *313*, 1270–1273.

(38) Bennici, S. M.; Vogelaar, B. M.; Nijhuis, T. A.; Weckhuysen, B. M. *Angew. Chem. Int. Ed.* **2007**, *46*, 5412–5416.

(39) Ferrari, A. C.; Robertson, J. *Phys. Rev. B* **2000**, *61*, 14095–14107.

(40) Hotta, M.; Hayashi, M.; Lanagan, M. T.; Agrawal, D. K.; Nagata, K. *Isij Int.* **2011**, *51*, 1766–1772.

(41) Karpov, A.; Dobner, C. K.; Glaum, R.; Schunk, S. A.; Rosowski, F. *Chem. Ing. Tech.* **2011**, *83*, 1697–1704.

(42) Grandin, A.; Chardon, J.; Borel, M. M.; Leclaire, A.; Raveau, B. *J. Solid State Chem.* **1993**, *104*, 226–231.

(43) Bauhofer, W. *J. Phys. E: Sci. Instrum.* **1981**, *14*, 934–938.

(44) Willinger, M. G.; Su, D. S.; Schlögl, R. *Phys. Rev. B* **2005**, *71*, 155118.

(45) Laubach, S.; Schmidt, P. C.; Thissen, A.; Fernandez-Madrigal, F. J.; Wu, Q. H.; Jaegermann, W.; Klemm, M.; Horn, S. *Phys. Chem. Chem. Phys.* **2007**, *9*, 2564–2576.

(46) Haber, J.; Witko, M. *J. Catal.* **2003**, *216*, 416–424.

(47) Ayyappan, P.; Ramanan, A.; Torardi, C. C. *Inorg. Chem.* **1998**, *37*, 3628–3634.

(48) Kang, H. Y.; Wang, S. L.; Tsai, P. P.; Lii, K. H. *J. Chem. Soc. Dalton Trans.* **1993**, 1525–1528.

(49) Glaum, R.; Welker-Nieuwoudt, C.; Dobner, C.-K.; Eichelbaum, M.; Gruchow, F.; Heine, C.; Karpov, A.; Kniep, R.; Rosowski, F.; Schlögl, R.; Schunk, S. A.; Titlbach, S.; Trunschke, A. *Chem. Ing. Tech.* **2012**, DOI: cite.201200078.

(50) Tietze, H. R. *Aust. J. Chem.* **1981**, *34*, 2035–2038.

(51) Binnewies, M.; Glaum, R.; Schmidt, M.; Schmidt, P. *Chemical Transport Reactions*, 1st ed.; Walter de Gruyter: Berlin, 2012.

(52) Glaum, R.; Gruehn, R. *Z. Kristallogr.* **1992**, *198*, 41–47.

(53) Knop-Gericke, A.; Kleimenov, E.; Hävecker, M.; Blume, R.; Teschner, D.; Zafeiratos, S.; Schlögl, R.; Bukhtiyarov, V. I.; Kaichev, V. V.; Prosvirin, I. P.; Nizovskii, A. I.; Bluhm, H.; Barinov, A.; Dudin, P.; Kiskinova, M. In *Advances in Catalysis*; Bruce, C. G., Helmut, K., Eds.; Elsevier Academic Press Inc, 2009; Vol. 52, Chapter 4 X-Ray Photoelectron Spectroscopy for Investigation of Heterogeneous Catalytic Processes, pp 213–272.

SUPPORTING INFORMATION:

Towards physical descriptors of active and selective catalysts for the oxidation of n-butane to maleic anhydride

Maik Eichelbaum,[*,†] Robert Glaum,[‡] Michael Hävecker,[†,¶] Knut Wittich,[‡] Christian Heine,[†] Heiner Schwarz,[†] Cornelia-Katharina Dobner,[§] Cathrin Welker-Nieuwoudt,[§] Annette Trunschke,[†] and Robert Schlögl[†]

Department of Inorganic Chemistry, Fritz-Haber-Institut der Max-Planck-Gesellschaft, Faradayweg 4-6, 14195 Berlin, Germany, Institut für Anorganische Chemie, Universität Bonn, Gerhard-Domagk-Straße 1, 53121 Bonn, Germany, Solar Energy Research, Helmholtz-Zentrum Berlin / BESSY II, Albert-Einstein-Straße 15, 12489 Berlin, Germany, and Chemicals Research and Engineering, BASF SE, Carl-Bosch-Straße 38, 67056 Ludwigshafen, Germany

E-mail: me@fhi-berlin.mpg.de

Phone: +49 (0)30 84134566. Fax: +49 (0)30 84134401

[*]To whom correspondence should be addressed
[†]Fritz-Haber-Institut
[‡]Universität Bonn
[¶]Helmholtz-Zentrum Berlin
[§]BASF SE

X-ray powder diffractometry

All measurements were performed at room temperature on a STOE Stadi-P transmission diffractometer using Cu Kα radiation. Shown are always the measured (blue line) and, if the crystal structures are known, calculated diffractograms (green line: after Rietveld refinement, anisotropic fit using 6th order spherical harmonics; red line: with corrected background) of the investigated samples. Additionally, the difference between observed and calculated background-corrected intensities are shown in gray. Calculated peak positions of the Bragg reflections are indicated as tick marks at the bottom of the graphs. In the right corners a representative excerpt of the accordant crystal structure is shown schematically, if known.

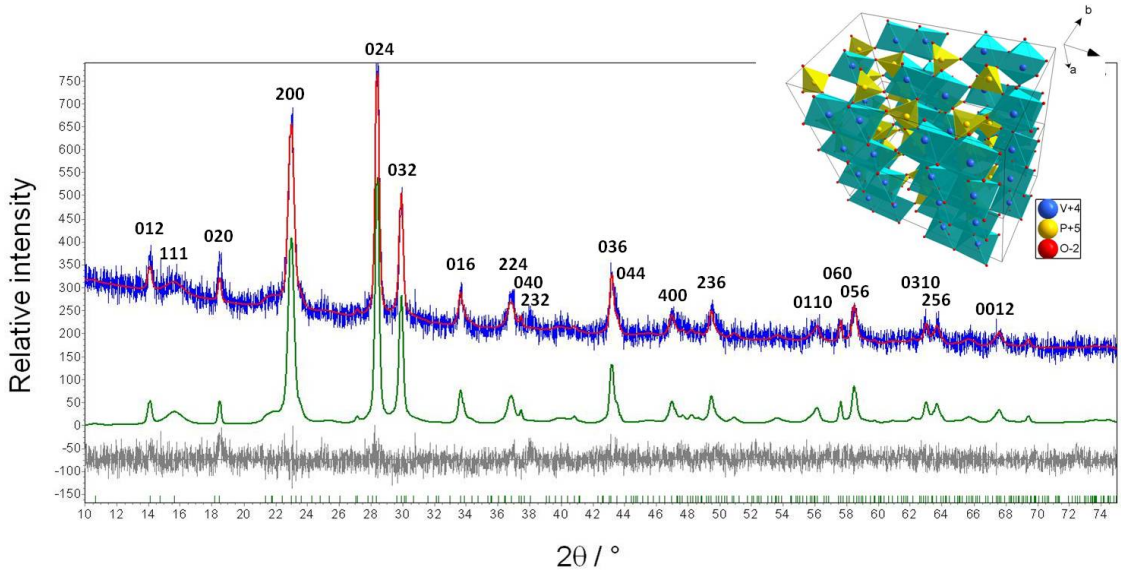

Figure S 1: $(V^{IV}O)_2P_2O_7$.

Table S 1: Lattice parameters and cell volumes of the VPP catalyst after treatment under n-butane oxidation reaction conditions ("as is"), after 2 h treatment in 5% H_2 in He at 400°C ("red") and after 2 h treatment in 5% O_2 in He at 400°C ("ox"), as determined by XRPD at 25°C in He.

Treatment	a [Å]	b [Å]	c [Å]	V [Å^3]
"as is"	7.734 ± 0.005	9.595 ± 0.004	16.610 ± 0.008	1233.0 ± 1.1
"red"	7.739 ± 0.005	9.595 ± 0.004	16.612 ± 0.008	1233.6 ± 1.1
"ox"	7.739 ± 0.005	9.594 ± 0.004	16.611 ± 0.008	1233.5 ± 1.1

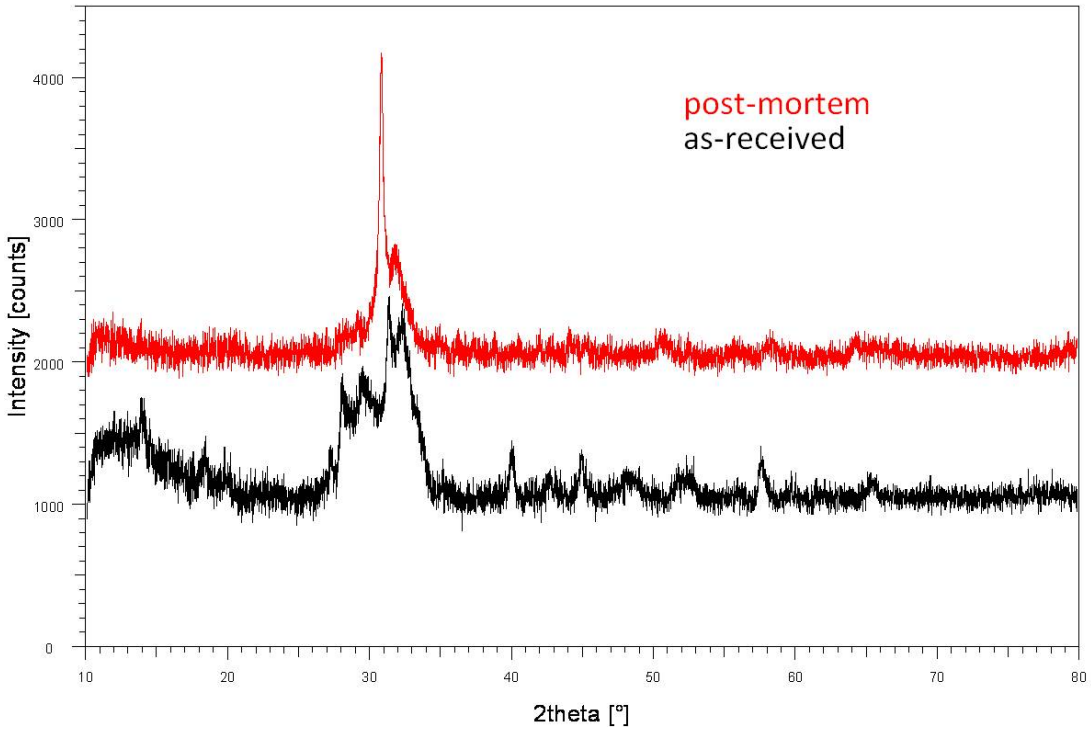

Figure S 2: $Ag_2V^{IV,V}P_{1.6}O_{7+\delta}$. The diffractograms of the sample before (as-received) and after the measurement cycle reported in the article (post-mortem) are depicted.

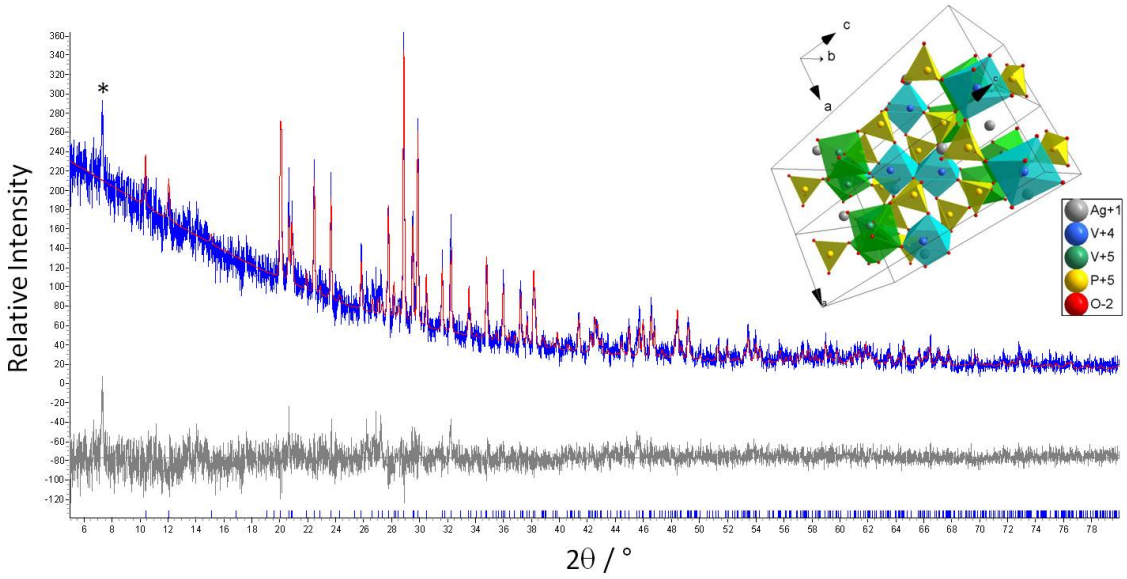

Figure S 3: $Ag(V^{IV}O)(V^{V}O)(PO_4)_2$. The reflex marked with "*" could not be assigned to this phase.

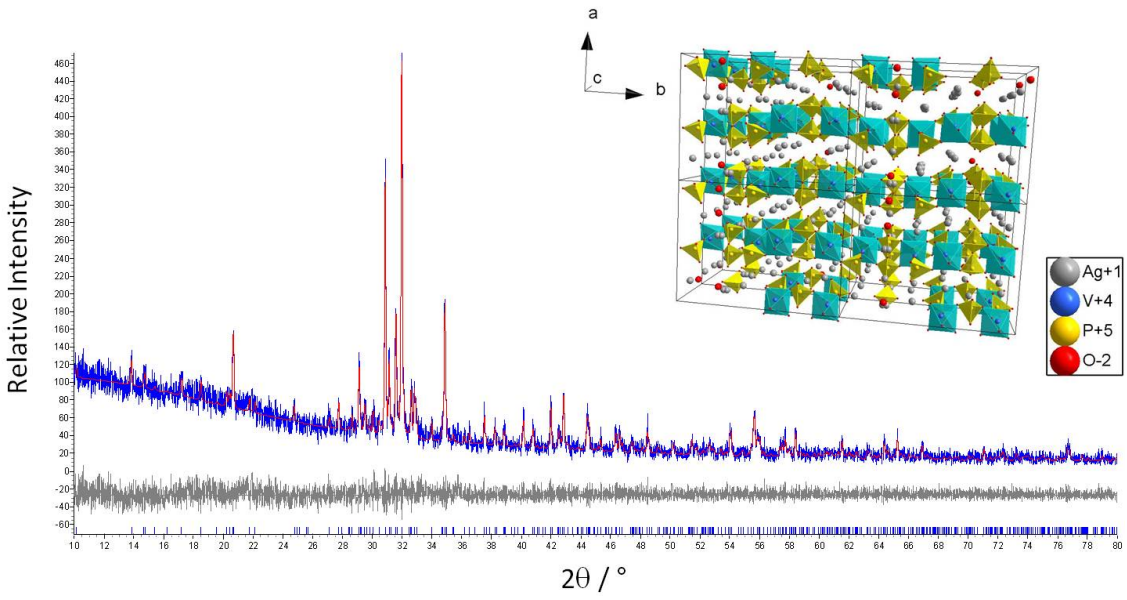

Figure S 4: $Ag_6(V^{IV}O)_2(PO_4)_2(P_2O_7)$.

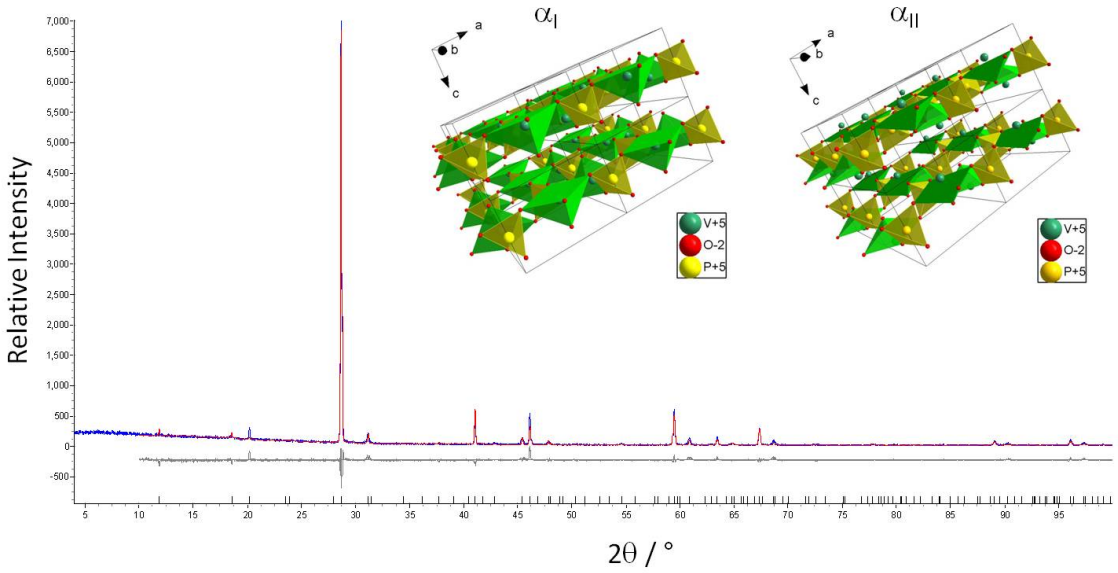

Figure S 5: α-$V^{V}OPO_4$/$V^{V}OPO_4 \cdot 2H_2O$. The α-phases and the dihydrate cannot easily be distinguished and reversibly transform into each other (by intercalation and extraction, respectively, of water between the layers) under the applied high temperature reaction conditions.

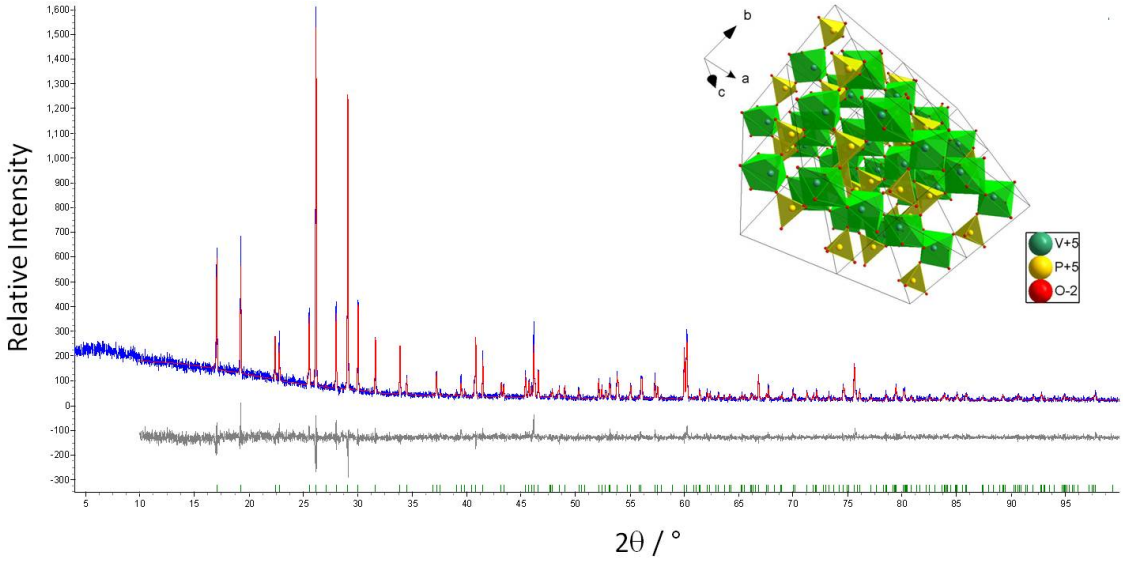

Figure S 6: β-$V^{V}OPO_4$.

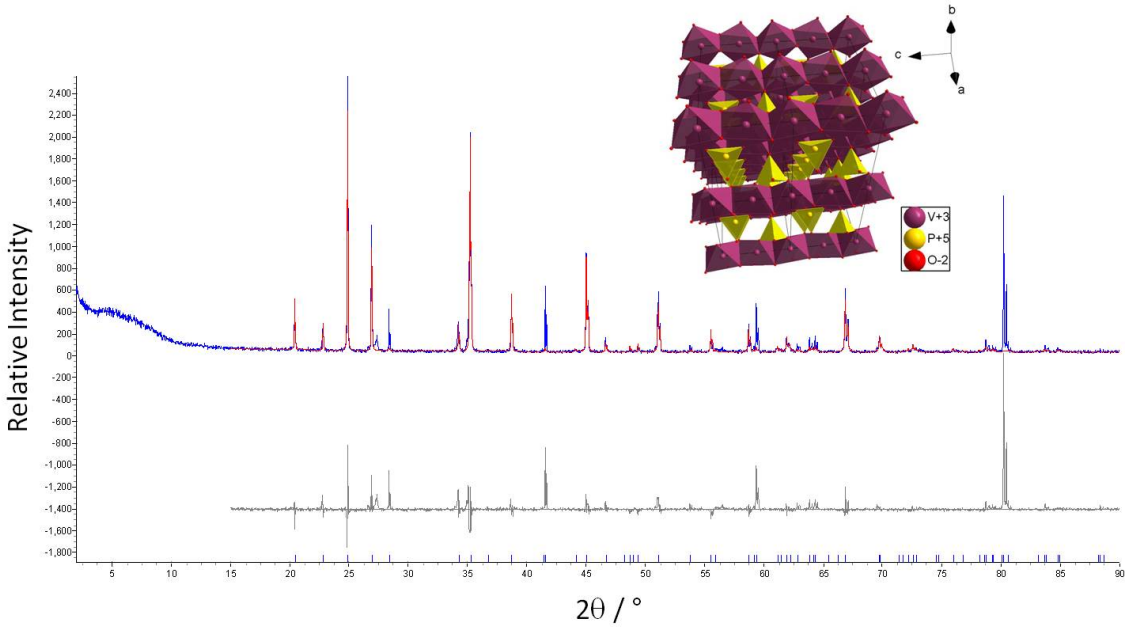

Figure S 7: $V^{III}PO_4$. The phase could be unambigously identified, however a meaningful fitting of the diffractogram was not possible due to strong predominant orientations in the crystal particles.